This article has been accepted for publication in IEEE Transactions on Plasma Science. This is the author's version which has not been fully edited and content may change prior to final publication. Citation information: DOI 10.1109/TPS.2022.3193348

MANUSCRIPT ID NUMBER: TPS14471

Numerical simulation of Helium arc at high pressure and low current

Avinash Maharaj, *PhD student, University of KwaZulu-Natal*, Oleg Kazak, *Application Engineer, Siemens Digital Industries Software*, Angelo Limone, *Technical Product Manager, Siemens Digital Industries Software*, Antonio D'Angola, *Professor, Università della Basilicata*, Gianpiero Colonna, *Senior Researcher, National Research Council (CNR)*, Yann Cressault, *Professor, Université de Toulouse III*, Samuel A. Iwarere, *Senior Researcher and Royal Society FLAIR Fellow, University of Pretoria and Honorary Research Fellow, University of KwaZulu-Natal*

***Abstract*— A Computational Fluid Dynamics (CFD) model has been developed to investigate the time evolution of a Helium plasma discharge at high pressures (from 2 - 8 MPa) and low electric current (0.35 A), including the interaction between the plasma and the electromagnetic fields, under Local Thermodynamic Equilibrium (LTE) assumption. To account for pressure dependence, novel thermodynamic and transport properties have been calculated in a wide pressure and temperature range. The model has been further improved by considering the effect of plasma-electrode interactions and the formation of the plasma sheath. High Performance Computing (HPC) was used to solve the CFD simulation, focusing on reference cases at 8 MPa and 0.35 A. Numerical results have shown that the sheath model and updated transport and thermodynamic properties have a significant impact on the electric potential, resulting in very good agreement between the simulation and experimental values.**

***Index Terms*— plasma, arc, reactor, simulation**

I. Introduction

A Computational Fluid Dynamics (CFD) model has been developed to simulate and investigate a plasma arc discharge. The model considers Helium gas at the unusual condition of high pressure (8 MPa), and a low current (0.35 A) applied to the cathode. These operating conditions are unique since investigations are typically performed in the pressure range of 0.01 – 0.1 MPa at high current (≥ 1 A) [1]. The simulation is performed using *Simcenter STAR-CCM+ version 2021.1* which is a commercial software, and the modelling approach is based on Lebouvier et al. [1].

In a view to investigate the effect of high pressure on the synthesis of hydrocarbons in Fischer-Tropsch application, a batch reactor with pressure capability of 20 MPa was developed. Discharges above 0.1 MPa and at low currents (< 1 A) have not been studied as extensively as discharges in the pressure range of 0.01 – 0.1 MPa and at high current (≥ 1 A) [1]. An explanation for this can be the technical and technological challenges to develop a reactor able to sustain and maintain a plasma at very high pressures. Therefore, to generate a discharge at such conditions, it is important to overcome the constraint of the Paschen law. In addition, the stability of reactive gases such as syngas requires the addition of an inert gas like Helium to enable the operation of the reactor to pressure above 2 MPa. Hence, the model simulates an experimental-based batch reactor working with Helium gas as a case study with the Helium considered as a non-reactive working gas. The purpose of this *Simcenter STAR-CCM+* CFD

This work was supported by South Africa's Centre for High Performance Computing (CHPC). As at the time of this write up, the corresponding author – Samuel A. Iwarere is funded by the Royal Society as a FLAIR Fellow [FLR\R1\201683].

The corresponding author is Samuel A. Iwarere (samuel.iwarere@up.ac.za).

Avinash Maharaj was the main author and responsible for the first draft of the manuscript. All authors provided review and comment on the subsequent versions of the manuscript. Avinash Maharaj was responsible for CFD simulations, analysis, and interpretation of results.

Oleg Kazak and Angelo Limone provided support, guidance and mentoring of the CFD simulation setup. They have also aided with interpretation of CFD results and provided the current-voltage characteristics for the metal-plasma interface.

Antonio D'Angola and Gianpiero Colonna provided suggestions to improve the mathematical model and the manuscript. They also performed the calculation of thermodynamic and transport properties of Helium plasma at different temperature and pressures using the *EquilTheTA* tool.

Yann Cressault has provided the Helium Net Emission Coefficient (NEC) for the pressure range which was investigated. He also provided input, review and editing towards the manuscript.

Samuel A. Iwarere was the main academic and research supervisor. He has provided support with the model setup, analysis, and interpretation of results. He also provided input, review and editing towards the manuscript.

All authors read and approved the final manuscript.

Avinash Maharaj is a part-time PhD student in the Discipline of Chemical Engineering, School of Engineering, University of KwaZulu-Natal, Howard College Campus, Durban, South Africa (e-mail: avimaharaj1@gmail.com).

Oleg Kazak is an Application Engineer at Siemens Digital Industries Software, 200 Shepherds Bush Road W6 7NL London, UK, (e-mail: oleg.kazak@siemens.com).

Angelo Limone is a Technical Product Manager at Siemens Digital Industries Software, 200 Shepherds Bush Road W6 7NL London, UK, (e-mail: angelolimone@gmail.com).

Antonio D'Angola is a Professor at Scuola di Ingegneria, Università della Basilicata, Potenza, Italy. He is also a Researcher at ISTP, National Research Council (CNR), Bari, Italy (e-mail: antonio.dangola@unibas.it).

Gianpiero Colonna is a Senior Researcher at ISTP, National Research Council (CNR), Bari, Italy (e-mail: gianpiero.colonna@cnr.it).

Yann Cressault is a Professor at Université de Toulouse, UPS, INPT, LAPLACE (Laboratoire Plasma et Conversion d'Energie), 118 route de Narbonne, F-31062 Toulouse Cedex 9, France (e-mail: cressault@laplace.univ-tlse.fr).

Samuel A. Iwarere is a Senior Researcher and Royal Society FLAIR Fellow at the Department of Chemical Engineering, University of Pretoria, Lynwood Road, Hatfield, Pretoria, South Africa. He is also an Honorary Research Fellow at the University of KwaZulu-Natal (e-mail: samuel.iwarere@up.ac.za).

© 2022 IEEE. Personal use is permitted, but republication/redistribution requires IEEE permission. See https://www.ieee.org/publications/rights/index.html for more information.

This article has been accepted for publication in IEEE Transactions on Plasma Science. This is the author's version which has not been fully edited and content may change prior to final publication. Citation information: DOI 10.1109/TPS.2022.3193348

model discussed in this study is to extend the findings of existing literature such as Lebouvier and co-workers by accounting for the following:

- Electrical characterization of the electrodes in the form of a sheath model.
- Improved thermodynamic and transport properties for Helium especially with regards to the specific heat.
- The Net Emission Coefficient (NEC) being specified at the individual operating pressures instead of a constant NEC at all pressures in literature. NEC above atmospheric pressure was previously unavailable in literature and our study provides new data for the plasma physics community.

The transport coefficients for Helium at high temperatures has been previously reported in literature by Murphy [2]. In the present study, thermodynamic and transport properties was calculated by using the *EquilTheTA* tool [3], [4], [5], [6], [7], [8] and [9], showing the significant dependence of the heat capacity and other thermodynamic quantities on temperature and pressure, improving the data used in the simulation conditions (pressure from 2 MPa up to 8 MPa and temperature up to 20000 K). The Net Emission Coefficient (NEC) for pure Helium was considered for the simulated pressure range [10, 11]. The simulations have been carried out assuming Local Thermodynamic Equilibrium (LTE).

The model considers the magnetohydrodynamic (MHD) effects, to include the interaction between the electrically conducting fluid (in this case a plasma) and electromagnetic fields, introducing also an electrode sheath model based on the empirical formula proposed by Rümpler [12]. The electric potential simulation results are compared against experimental measurements in the investigated pressure range.

In Section 2, the CFD model has been introduced and fully described, highlighting the coupling between Maxwell equations and the continuity, momentum, and energy equations. In Section 3, details on the boundary conditions, thermodynamic and transport properties, the radiation, and the sheath model have been reported, while in Section 4 the meshing procedure have been presented. Finally, in Sections 5 and 6 numerical results have been presented and discussed together in comparison with experimental data.

The outcomes from this research will provide a deeper understanding of the complex electric field conditions and fluid dynamic effects which are prevalent in a plasma discharge especially at pressures greater than 1 MPa. The results could provide an opportunity for the redesigning of the arc discharge reactor for potential environmental applications.

II. Computational Fluid Dynamics (CFD): Computational Domain and Mathematical Model

A two-dimensional view of the computational domain is shown in Fig. 1. The electrode configuration is pin-to-plane with 1 mm gap and grounded anode. The reactor is positioned horizontally with the coordinate system shown in Fig. 1 at the bottom left-hand side. The plasma arc CFD model is based on the Eulerian approach with the fluid flow and electromagnetism governing equations coupled together for the application The fluid flow and electromagnetism governing equations have been taken from the theory section of the *Simcenter STAR-CCM+* user manual, the commercial software that was used for the numerical simulation [13].

A. Assumptions

The time-dependent mathematical model is based on the following main assumptions which have been adopted from Lebouvier et al. [1]:

- The Helium plasma is considered as a single continuous fluid.
- The plasma was assumed to be at Local Thermodynamic Equilibrium (LTE).
- The gravitational force is included and acts in the negative *x* direction as per the coordinate system in Fig. 1.

The Helium gas flow is laminar. Preliminary calculations showed that a low Reynolds number (less than 10) can be expected in the inter-electrode region of the reactor. This motivated the selection of the laminar flow model for the simulation.

B. Fluid flow governing equations

The conservation equations for mass, linear momentum, and energy are given by (1), (2) and (3) respectively.

$$\frac{\partial \rho}{\partial t} + \boldsymbol{\nabla} \cdot (\rho \mathbf{v}) = 0 \tag{1}$$

Where:

ρ = Density
t = Time
$\mathbf{v}$ = Velocity

$$\frac{\partial (\rho \mathbf{v})}{\partial t} + \boldsymbol{\nabla} \cdot (\rho \mathbf{v} \otimes \mathbf{v}) = \boldsymbol{\nabla} \cdot \mathbf{C} + \mathbf{f}_g + \mathbf{f}_{\mathrm{L}} \tag{2}$$

For a fluid, the stress tensor ($\mathbf{C}$) is expressed as the sum of the normal stresses and shear stresses, $\mathbf{C} = -p\mathbf{I} + \mathbf{T}$, where p is the pressure, $\mathbf{I}$ is the moment of inertia and $\mathbf{T}$ is the viscous stress tensor.

Where:

$\mathbf{f}_g$ = Gravitational force per volume unit acting on the Helium gas
$\mathbf{f}_{\mathrm{L}}$ = Lorentz force per volume unit acting on the Helium gas

© 2022 IEEE. Personal use is permitted, but republication/redistribution requires IEEE permission. See https://www.ieee.org/publications/rights/index.html for more information.

This article has been accepted for publication in IEEE Transactions on Plasma Science. This is the author's version which has not been fully edited and content may change prior to final publication. Citation information: DOI 10.1109/TPS.2022.3193348

$$\frac{\partial(\rho E)}{\partial t} + \nabla \cdot (\rho E \mathbf{v}) = (\mathbf{f}_g + \mathbf{f}_\mathrm{L}) \cdot \mathbf{v} + \nabla \cdot (\mathbf{v} \cdot \mathbf{C}) - \nabla \cdot \mathbf{q} - S_E + Q \quad (3)$$

Where:

E	=	Total energy per unit mass
$\mathbf{q}$	=	Diffusive heat flux
S_E	=	An energy sink term (i.e., the radiation loss calculated using the Net Emission Coefficient (NEC))
Q	=	An energy source term (i.e., the heat generated by Joule / Ohmic heating)

C. Electromagnetism governing equations

The fluid flow and electromagnetism governing equations are coupled due to the temperature and pressure dependence of thermodynamic properties and the electrical conductivity transport property.

The electromagnetic phenomena must be accounted for in the simulation because it describes the interaction between electrically charged particles in terms of electric fields, magnetic fields, and their mutual interaction. The fundamental laws that describe the electromagnetic behavior of a fluid are Maxwell's equations and the conservation of electric charge. Maxwell's equations can be written as:

$$\frac{\partial \mathbf{B}}{\partial t} + \nabla \times \mathbf{E} = 0 \quad (4)$$

$$\frac{\partial \mathbf{D}}{\partial t} - \nabla \times \mathbf{H} = -\mathbf{J} \quad (5)$$

$$\nabla \cdot \mathbf{D} = \rho_e \quad (6)$$

$$\nabla \cdot \mathbf{B} = 0 \quad (7)$$

Where:

$\mathbf{B}$	=	Magnetic flux density
$\mathbf{E}$	=	Electric field
$\mathbf{D}$	=	Electric flux density
$\mathbf{H}$	=	Magnetic field
$\mathbf{J}$	=	Electric current density
ρ_e	=	Charge density

The conservation of charge within a control volume is given by the continuity equation:

$$\nabla \cdot \mathbf{J} + \frac{\partial \rho_e}{\partial t} = 0 \quad (8)$$

It is worth noting that a magnetohydrodynamics (MHD) formulation was used. The *Simcenter STAR-CCM+* MHD formulation does not include charge accumulation, so the local charge density (ρ_e) is always zero.

a. Magnetohydrodynamics (MHD) and the generalized Ohm's law

Magnetohydrodynamics (MHD) describes the interaction between electrically conducting fluids (such as plasma) and electromagnetic fields. A conducting fluid in relative motion to a magnetic field induces an electric current density ($\mathbf{J}_\mathrm{L}$). This induced electric current density ($\mathbf{J}_\mathrm{L}$) contributes to the total electric current density ($\mathbf{J}$). The generalized Ohm's law is then given by:

$$\mathbf{J} = \sigma \mathbf{E} + \mathbf{J}_\mathrm{L} = \sigma(\mathbf{E} + \mathbf{v} \times \mathbf{B}) \quad (9)$$

Where σ is the electrical conductivity and $\mathbf{v}$ is the flow velocity of the fluid.

The conducting fluid experiences a body force per unit volume known as the Lorentz force ($\mathbf{f}_\mathrm{L}$) and is described by (10). This Lorentz force will influence the motion of the gas in the reactor and consequently the velocity field.

$$\mathbf{f}_\mathrm{L} = \mathbf{J} \times \mathbf{B} \quad (10)$$

b. Potential formulation of the governing equations

When using the two-way coupled MHD approach, the Maxwell equations (4) and (7) can be reformulated in terms of two auxiliary fields, the electric scalar potential (ϕ_e) and the magnetic vector potential ($\mathbf{A}$), as shown in in the following:

$$\mathbf{E} = -\nabla \phi_e - \frac{\partial \mathbf{A}}{\partial t} + \mathbf{v} \times \mathbf{B} \quad (11)$$

$$\mathbf{B} = \nabla \times \mathbf{A} \quad (12)$$

Reformulating Maxwell's equations in terms of the potentials reduces the number of independent equations, because (4) and (7) become identities. However, the potentials are not unique. To uniquely define the magnetic vector potential $\mathbf{A}$, it becomes necessary to prescribe both its curl and divergence. The divergence of $\mathbf{A}$ is defined by the Coulomb gauge condition, $\nabla \cdot \mathbf{A} = \mathbf{0}$.

When (11) is substituted into (9), Ohm's law can be written in terms of the electric scalar and magnetic vector potentials as:

$$\mathbf{J} = -\sigma \nabla \phi_e - \sigma \frac{\partial \mathbf{A}}{\partial t} + \mathbf{J}_\mathrm{L} \quad (13)$$

© 2022 IEEE. Personal use is permitted, but republication/redistribution requires IEEE permission. See https://www.ieee.org/publications/rights/index.html for more information.

This article has been accepted for publication in IEEE Transactions on Plasma Science. This is the author's version which has not been fully edited and content may change prior to final publication. Citation information: DOI 10.1109/TPS.2022.3193348

Electromagnetics in conducting fluids

For fields that vary with time, the magnetic and electric fields are mutually coupled. The displacement and conduction currents associated with the electric field contribute to the magnetic field as per (5). The formulation considers low-frequency electromagnetic fields in conducting fluids, where the conduction currents are several orders of magnitude greater than the displacement currents, i.e., $\mathbf{J} \geq \frac{\partial \mathbf{D}}{\partial t}$. Neglecting the displacement currents reduces (5) to Ampere's law:

$$\nabla \times \frac{1}{\mu_0}\mathbf{B} = \mathbf{J} \tag{14}$$

Where μ_0 is the magnetic permeability and describes the behavior of the fluid in response to a magnetic field. The magnetic permeability also describes the constitutive relation between the magnetic field (**H**) and magnetic flux density (**B**).

$$\mathbf{B} = \mu_0 \mathbf{H} \tag{15}$$

The constitutive relation in (15) can be used because the simulation does not include any ferromagnetic materials.

Additionally for conducting fluids, the divergence of the electric current density **J** is zero because there is no charge accumulation, and (8) reduces to:

$$\nabla \cdot \mathbf{J} = 0 \tag{16}$$

(12), (13) and (15) can be substituted into (14) and (16) to form the following:

$$\nabla \times \frac{1}{\mu_0}\nabla \times \mathbf{A} + \sigma \frac{\partial \mathbf{A}}{\partial t} = -\sigma \nabla \phi + \mathbf{J}_{\mathrm{L}} \tag{17}$$

$$-\nabla \cdot (\sigma \nabla \phi) = \nabla \cdot \left(\sigma \frac{\partial \mathbf{A}}{\partial t}\right) + \nabla \cdot \mathbf{J}_{\mathrm{L}} \tag{18}$$

(17) and (18) describe the response of a conducting fluid to low-frequency electromagnetic fields. These are a set of mutually coupled equations with two unknown fields, **A** and ϕ, which are solved using two separate solvers.

c. Joule heating

Joule heating (also referred to as Ohmic heating) describes the relationship between electric currents and temperature changes in conducting materials. It is an important principle in plasma simulations since the arc is ignited by the Ohmic heating generated in the conductive region. Joule's law states that the heat source per unit volume (Q) due to an electric current density (**J**) is given by

$$Q = \frac{\mathbf{J}^2}{\sigma} \tag{19}$$

III. Simulation Setup

The model outlined above is applied to describe an arc type discharge. Local Chemical Equilibrium (LCE) can be assumed because the plasma reactions occur at a time scale which is much lower than the one considered for the arc dynamics, allowing to define the thermodynamic and transport properties of the plasma as a function of temperature and pressure. The assumption of Local Thermodynamic Equilibrium (LTE) also applies which states that the electron temperature is equal to the heavy species gas temperature. The electrons can remain in thermal equilibrium with the gas temperature due to collisions at the considered pressure and density. The plasma interacts with cold gas streams, and other phenomena such as thermionic emission can occur at the cathode. In these regions, the assumption of LTE is not more valid and due to non-equilibrium effects, the electron temperature is far from the gas temperature.

The electrode and plasma regions have been defined individually as three-dimensional substances. In fact, although the geometry is inherently two dimensional – axisymmetric, the physics is not due to the off-axis gravity.

A coupled solver is used to solve the fluid flow and electromagnetism equations in a coupled manner, simultaneously as a vector of equations. The velocity field is obtained from the momentum equation, the pressure is determined from the conservation of mass equation and the density is evaluated from the equation of state.

The time step is set to 0.25 μs for the first 2 ms of the simulation to ensure the stability of the simulation and discharge. Thereafter the time step is set to 1 μs up to a physical time of 50 ms. This time step is much lower than the typical value of 5μs used for plasma modelling [14, 15]. A lower time step was used to ensure convergence of the simulation.

The Reynolds numbers will remain low in the reactor and therefore the flow will remain in the laminar viscous regime.

The electrode material is defined as being copper and the electrical conductivity is specified as 5.96×107 S/m. Although copper is a non-refractory material unlike tungsten, which is commonly used in arc welding applications, the work function of both materials is very close (copper being 4.46 eV and tungsten 4.5 eV) and a simulation using both materials present a result of (± 1 K and ±1 V) for the temperature and electric potential respectively.

A. Boundary conditions

Correct specification of the boundary conditions is vital in achieving accurate results. All boundaries have been defined as walls. A wall boundary represents an impermeable surface which confines the solid (electrodes) and fluid (Helium plasma) regions. The cathode and anode boundaries are defined by AB

© 2022 IEEE. Personal use is permitted, but republication/redistribution requires IEEE permission. See https://www.ieee.org/publications/rights/index.html for more information.

This article has been accepted for publication in IEEE Transactions on Plasma Science. This is the author's version which has not been fully edited and content may change prior to final publication. Citation information: DOI 10.1109/TPS.2022.3193348

and CD respectively as shown in Fig. 1. The electrode magnetic field boundary conditions are imposed far from the arc and therefore do not have an artificial influence on the Lorentz force.

The boundary conditions for the simulation are given in Table I. The electrode and Helium boundary conditions are explained more specifically in the following sub sections.

a. Electrode boundary conditions

The cathode boundary *AB* satisfies the Neumann boundary condition, which defines the component of the electric scalar potential gradient ($\nabla\phi_e$) orthogonal to the boundary. The cathode boundary condition has been defined by specifying the total electric current (I) through *AB*.

The anode electric potential boundary *CD* satisfies the Dirichlet boundary conditions. The electric scalar potential (ϕ_e) is specified at *CD*.

The cathode and anode walls electric potential boundaries are considered insulators and, consequently, the total electric current through the boundary is set to zero.

The cathode and anode magnetic vector potential boundary condition sets the tangential component of the magnetic vector potential $\left(\mathbf{A}_{tangent}\right)$ to zero whilst leaving the normal component free. Finally, the electrode boundary conditions have been summarized in Table II.

b. Helium boundary conditions

The entire Helium boundary is considered as a wall. The no-slip shear stress condition has been specified. For a no-slip wall, the fluid moves at the same velocity as the wall, i.e., the fluid velocity relative to the wall velocity is zero. The tangential velocity is specified as being fixed, therefore $\mathbf{v}_{\text{wall}} = 0$, where $\mathbf{v}_{\text{wall}}$ is the wall fluid velocity. In this case the wall static pressure $\left(p_{static,wall}\right)$ is zero.

The computation of the wall fluid temperature depends on the thermal specification of the wall. The thermal specification for the Helium wall boundary has been specified as adiabatic (i.e., heat transfer is not permitted across the boundary). Static temperature, density and total enthalpy at the wall are extrapolated (ext) from the interior of the domain and equal to

$$\begin{aligned} T_{static,wall} &= T_{static}^{ext} \\ \rho_{static,wall} &= \rho_{static}^{ext} \\ H_{total,wall} &= H_{wall}^{ext} \end{aligned} \tag{20}$$

The adiabatic condition can be specified because an energy sink using the NEC has been defined. A steady state of the plasma can then be achieved due to the energy balance between the input energy (Ohmic heating) and output energy (NEC).

The Helium wall boundaries are defined as being insulators. The magnetic vector potential boundaries set the tangential component of the magnetic vector potential $\left(\mathbf{A}_{tangent}\right)$ to zero whilst leaving the normal component free. Finally, the Helium boundary conditions have been summarized in Table III.

c. Thermodynamic and transport properties

Thermodynamic properties (i.e., enthalpy (H), density (ρ) and specific heat $\left(C_p\right)$ and transport coefficients (i.e., dynamic viscosity (μ), electrical conductivity (σ), and thermal conductivity (λ)) of plasmas are important input data to achieve accurate CFD results. In this instance it is possible to carry out the modelling assuming LCE by defining the plasma with two independent state variables such as pressure and temperature [4]. Gupta et al. [16] made the same assumption of LCE to obtain thermodynamic and transport properties for equilibrium air up to 30 000 K.

The *EquilTheTA* tool [3], [4] was used in this study to update the thermodynamic and transport properties, especially the specific heat capacity, in the high pressure (up to 8 MPa) and high temperature (up 20000 K) ranges to improve the accuracy of numerical results. *EquilTheTA* is based on an approach which consists in solving one equilibrium equation at a time [5], [6], [7], [8], [9], [17], and calculates chemical equilibrium, thermodynamic properties and transport coefficients starting from recent and accurate databases of atomic and molecular energy levels and collision integrals.

The thermodynamic properties of enthalpy (Fig. 2) and specific heat at constant pressure (Fig. 3) are mainly affected by the population of the excited levels and ion concentration. Due to the very large energy of the first Helium excited state ($\sim$ 20 eV), the molar enthalpy is given by 1.5 RT and the molar specific heat is 2.5 R, which is valid up to $T \sim$ 12000 K. The enthalpy and specific heat do not depend on the pressure for this temperature range. R is the gas constant and T is the temperature.

For higher temperatures, the population of excited states and of ions becomes appreciable and these quantities grow. The thermodynamic properties then depend on pressure due to variation of the ionization degree and the cutoff for the energy levels (higher the pressure, lower the ionization degree and higher the cutoff). This behavior can also be observed on the density profile (Fig. 4).

Regarding the transport properties, the electrical conductivity (Fig. 5) is governed by the electron density becoming appreciable when it becomes large enough. For $T <$ 12000 K, the thermal conductivity (Fig. 6), related to the enthalpy, is mainly given by the translational contribution. The internal, reactive, and free electron contributions become appreciable at higher temperatures.

On the other hand, the dynamic viscosity (Fig. 7) is determined by the heavy particle density because electrons do not contribute. Therefore, the variation of the dynamic viscosity with the pressure is observed only at high temperature ($T >$ 16000 K).

© 2022 IEEE. Personal use is permitted, but republication/redistribution requires IEEE permission. See https://www.ieee.org/publications/rights/index.html for more information.

This article has been accepted for publication in IEEE Transactions on Plasma Science. This is the author's version which has not been fully edited and content may change prior to final publication. Citation information: DOI 10.1109/TPS.2022.3193348

d. Electrical conductivity constraint and the initial hot channel

When modelling the electric currents in conducting materials, the electrical conductivity (σ) defines the relationship between the electric current density (**J**) and the electric field (**E**) according to Ohm's law. In plasma arc simulations, the Ohmic Heating energy model heats the plasma. However, modelling an electric current through an electrically insulating gas at room temperature causes numerical instability due to the large scale of Ohmic heating and a low initial electrical conductivity.

To overcome this obstacle, an artificial electrical conductivity (AEC) channel in the Helium region was defined. This channel allowed for the electrical conductivity to be artificially raised by specifying a minimum electrical conductivity which allowed for the ignition of an electrical arc. The current flowing through this artificial channel heats up the gas so that the gas conductivity soon exceeds the artificial minimum conductivity. Such approaches to ignite the arc have also been used by Bernardi et al. [17], Chine [18], [19] and Fuchs et al. [20].

The electrical conductivity (σ) for Helium at 8 MPa shows that $\sigma \leq 1$ S/m when $T < 9200$ K. Therefore, the flow of electric current is not guaranteed by using LTE near the cooled anode wall. The use of an AEC overcomes this problem. The AEC channel is defined as a cylinder with a diameter of 0.2 mm and length of 3 mm and is positioned in the inter-electrode region. A local cylindrical coordinate system was created to assist with the AEC definition using a field function. This function states that σ = 1 S/m in the AEC channel and 4.766×10-20 S/m elsewhere in the computational domain.

The arc is further stabilized during the initial iterations by specifying an initial hot channel (IHC) as an initial condition for the Helium region. Initial conditions specify the initial field data for the simulation. The IHC was created using the same procedure as the AEC channel. The IHC is positioned between the electrodes and has a length of 1 mm. A field function was used to define the initial temperature which states that T = 15300 K (corresponds to σ = 847.48 S/m) in the IHC and 300 K (σ = 4.766×10-20 S/m) elsewhere in the computational domain.

e. Radiation losses

Thermal radiation can be defined as electromagnetic radiation emitted by matter in a state of thermal excitation [21]. Radiation transfer is the main mechanism of ensuring energy balance within a plasma arc [22]. The importance of thermal radiation in modelling physical problems increases with a raise in temperature. When temperatures are typically in the thousands of degrees Kelvin, the role of thermal radiation is primarily one of transmitting energy. When considering thermal radiation in a physical problem, the radiative properties of the matter must be known.

Exact calculations of radiation properties are very complex and time consuming, so it is desirable to account for radiation losses in an approximate manner. Net Emission Coefficients (NEC) are widely used in CFD simulations and are based on the assumption of Local Thermodynamic Equilibrium [23]. The use of NEC allows the simulation to pre-compute the energy balance within the arc among emitted, self-absorbed, and radiated energy. Therefore, it provides an estimation of the net radiation lost by the arc, by assuming a simple shape and current-dependent size for the arc.

Lowke [24] found that the approximation of arc temperature profiles using the Net Emission Coefficient (NEC) yields central arc temperatures and electric field strengths for a given arc to be accurate to 10%. The computational time for the approximate calculations was found to be more than an order of magnitude less compared to the calculation in which the radiation transfer was treated exactly. Billoux et al. [25] and Bartlova et al. [22] have shown in their work that the NEC is a good approximation to use in numerical modelling in order to characterize the radiation losses in hot regions while taking into consideration the absorption.

The data for the Helium NEC values used in the simulation are provided at 2, 4, 6 and 8 MPa in Fig. 8 [10]. The isothermal plasma sphere radius (R_p) is considered to be 1 mm, since this is the expected order of magnitude of the diameter of the simulated arc. The radiation losses using the NEC are accounted for by specifying an energy sink for the Helium gas.

f. Electrical characterization of the electrodes

Yokomizu et al. [26] performed experimental analysis to determine the electrode sheath voltages for Helium arcs up to a pressure of 0.1 MPa with AC currents between 330 A and 550 A. Electrodes made of iron, copper and titanium were used in the reactor. The inter-electrode gaps ranged between 0.2 and 3 mm. It was found that the electrode sheath voltages were independent of the electrode material.

Mentel et al. [27] used a model lamp to support modelling of the electrodes in high intensity discharge lamps. The investigation considered electrodes made from pure and modified tungsten. The investigations were performed in a current range between 1 – 10 A. The electrodes were operated in Argon or Xenon in a pressure range between 0.1 – 1 MPa.

Mentel et al. [27] stated that the current transfer between the cathode and the lamp plasma is much more complicated than that between the anode and the plasma. A power source is contained within a thin sheath in front of the cathode together with an electron current to the plasma column. This ion current balances the insufficient electron emission to the cathode. The power supply to the cathode by ions is the main reason for the cathode voltage drop.

Roth [28] and Fulcheri et al. [29] showed that an arc discharge can be split into three main domains: the near-cathode zone, the positive arc column and the near-anode zone as shown in Fig. 9. In the positive arc column, the density of the negative charges is equal to that of the positive charges, whereas in the border zones (near-cathode and near-anode zones), these two

© 2022 IEEE. Personal use is permitted, but republication/redistribution requires IEEE permission. See https://www.ieee.org/publications/rights/index.html for more information.

This article has been accepted for publication in IEEE Transactions on Plasma Science. This is the author's version which has not been fully edited and content may change prior to final publication. Citation information: DOI 10.1109/TPS.2022.3193348

densities can strongly differ. The plasma increasingly deviates from equilibrium conditions closer to the near-cathode and near-anode zones. The result is a strong difference in electrical behaviour between these zones. Fig. 9 shows the axial variation of the voltage drop varies quasi-linearly in the positive arc column while it is strongly non-linear in the near electrode zones.

The discharge voltage (U) is expressed as the sum of the positive arc column voltage drop (U_{column}), near-cathode $(U_{near-cathode})$ and near-anode voltage drops $(U_{near-anode})$

$$U = U_{column} + U_{near-cathode} + U_{near-anode} \tag{21}$$

In most instances the near-cathode voltage drop is larger than the near-anode voltage drop. The total characteristic length of the near-electrode zones will vary between 0.1 and 1 mm depending on the gas nature and pressure. A higher pressure typically reduces the thickness of the near-electrode zone. The thickness is independent of the inter-electrode gap whereas the arc column length depends on this gap.

The following empirical formula proposed by Rümpler [12] was used to define the near-cathode and near-anode voltage drop

$$\phi_e(|\mathbf{J}|) = \frac{a|\mathbf{J}| + b|\mathbf{J}|^d}{c + |\mathbf{J}|^d} \tag{22}$$

in which coefficients a, b, c, d are defined in Table IV [12]. The values are graphically represented in Fig. 10. The coefficients are for a gas at atmospheric pressure and were used in this modelling due to a lack of experimental data for the specific conditions being investigated.

An interface is specified between the solid (electrodes) and fluid (Helium plasma) regions during the simulation setup. This interface allows for simulation quantities (i.e., mass, momentum, energy, electromagnetism, etc.) to pass from one region to another. A coupled solver is used to solve the fluid flow and electromagnetism equations in a coupled manner, simultaneously as a vector of equations. The sheath model for both cathode and anode are defined at their respective interfaces. The Rümpler empirical formula is then used to specify the relationship between the voltage and electrical resistance at the interface between the electrodes and Helium plasma. The temperature inside the solid electrodes is not solved in this CFD model.

IV. Mesh Study

The construction of the volume mesh has a direct influence on the accuracy of the fluid flow and energy calculation, as well as the rate of convergence. The mesh has been designed to achieve adequate resolution in regions where spatial gradients are high. For this reason, the mesh is refined in the inter-electrode gap since this is the physical space where the plasma arc is initially ignited.

The volume mesh was generated using polyhedral cells which had a cell base size of 0.1 mm. The prism layer mesh model was used in conjunction with the polyhedral cells to generate orthogonal prismatic cells next to wall surfaces and boundaries. The prism layers are necessary to improve the accuracy of the flow simulation since they can capture viscous and thermal gradients close to the wall. The ability to resolve near wall flow accurately is critical in determining the forces and heat transfer on walls, as well as flow features such as separation, which in turn affects the pressure drop.

The prism layers consisted of two layers with a total thickness corresponding to 10% of the cell base size. A volumetric control in the form of a cylinder was used in the inter-electrode gap to achieve a smaller cell base size in this region. The cylinder was created with a diameter of 2 mm and length of 1 mm. The volumetric control contained a cell size corresponding to 10% of the base size. The generated mesh can be viewed in Fig. 11.

A mesh sensitivity analysis was performed to ensure that the results are independent of the mesh. High Performance Computing (HPC) was used to solve the CFD simulation. HPC is necessary in the analysis of the plasma arc simulation as it allows the problem to be investigated within a realistic time scale [30]. All simulations were performed on the Lengau cluster located at South Africa's Centre for High Performance Computing (CHPC) on ten virtual nodes, each with 24 cores running 24 message passing interfaces (MPI) processes.

V. Results

The results obtained from the plasma arc simulation is presented in this section.

A. Validation and verification

The simulation results have been validated against experimental measurements. The experimental electrical characterization was conducted in a tip-to-plane electrode configuration in a reactor chamber with capability of up to 20 MPa. The reactor is equipped with a K-type thermocouple to measure the temperature in the reactor and a water-cooling jacket. The reactor is powered by a Technix high voltage power supply, which is current controlled and set at an ignition voltage of 9 kV. The operating current is set on the power supply unit and can be measured using a Chauvin hall effect current clamp, while the voltage can be measure using an Elditest 30-kV high voltage probe, connected to the Wave Jet 3540A digital oscilloscope via BNC connect cables from the current and voltage probes. The helium gas is filled into the reactor from the helium baseline 5.0 cylinder to achieve the operating pressure. The helium gas cylinder was purchased from Afrox, with a minimum purity of 99.999%.

Fig. 12 shows the simulated electric potential from this study and the results from Lebouvier et al. [1] being compared with experimental results (10% uncertainties as shown by the error bars). The simulated electric potential measurements were obtained at the cathode tip. The results from this study are in

© 2022 IEEE. Personal use is permitted, but republication/redistribution requires IEEE permission. See https://www.ieee.org/publications/rights/index.html for more information.

This article has been accepted for publication in IEEE Transactions on Plasma Science. This is the author's version which has not been fully edited and content may change prior to final publication. Citation information: DOI 10.1109/TPS.2022.3193348

closer agreement with the experimental values when compared with the results from Lebouvier et al. [1]. It can be observed that as the pressure increases, the results from this study underestimated the electric potential when compared to the experimental results. Differences arise due to the empirical sheath model which is not yet fully ideal and results in a deviation from the experimental electric potential. Benilov [31] has stated that the existence of LTE even in the region of plasma near the cathode in a low current high-pressure arc is far from certain. Therefore, the slight difference between our simulation and the experimental data probably arise due to non-equilibrium effects since this deviation from LTE in the sheath region could be strong at low-current and impact on the electric potential at the higher pressure. Furthermore, the Rümpler empirical formula is defined for a gas at atmospheric pressure but was used in this study for the entire pressure range due to the lack of an empirical formula at high pressure.

The electric potential results from this study are larger than that from Lebouvier et al. [1] for the entire pressure range. The improved thermodynamic and transport properties from the *EquilTheTA* tool, the NEC being specified at the individual operating pressures, and the definition of the electrode sheath model, is responsible for the increased electric potential calculation.

B. The arc temperature and electric potential evolution

Fig. 13 shows the arc temperature evolution for the 8 MPa simulation. The high temperature region of the discharge extends from the cathode tip to the anode at a physical time of 2 ms. The cathode arc root remains attached to the cathode tip, whereas the anode arc root begins to slide along the anode after a physical time of 15 ms. Since the Helium density varies with temperature, the gravity vector acts on the density and induces a natural convection flow to the top of the reactor, which causes the bending of the arc. The arc shape after 50 ms is a result of the combined effects of the Lorentz force, gravity force and convection.

A representation of the entire electric potential domain and the evolution of the electric potential at the cathode tip for the 8 MPa simulation is shown in Fig. 14. The electric potential evolution shows that the value initially drops to a value of circa -270 V. Then the potential stabilizes at a value of -143 V. The electric potential is influenced by the Helium gas temperature increase, which causes a higher electrical conductivity. Fig. 15 shows the variation of the electric potential in the inter-electrode region at 8 MPa. A linear electric potential drop is observed.

C. Velocity fields in the reactor

Preliminary calculations revealed that a low Reynolds number (less than 10) can be expected in the inter-electrode region of the reactor. This motivated the selection of the laminar flow model for the simulation. The evolution of the velocity field in the reactor at 8 MPa is shown in Fig. 16.

Since a batch reactor is being investigated, the convective motion of the gas is fully dependent on natural convection. This implies a low velocity magnitude and a long time for the flow to be fully established. At a physical time of 2 ms, the maximum velocity region is located at the cathode tip. At 15 ms, the motion of the gas begins to move towards the top of the reactor. At a physical time of 15 ms, the gas reaches a maximum velocity magnitude of 1.27 m/s and the gas moves fully towards the top of the reactor. As the gas moves upwards it mixes with the cooler surrounding gas in the reactor, the gas temperature then lowers, and the gas moves towards the bottom and sides of the reactor as a result of the convection effect.

D. Electric current density

The electric current density magnitude ($|\mathbf{J}|$) at a physical time of 50 ms for the 8 MPa simulation is given in Fig. 17. A maximum value of 2.99×107 A/m2 is calculated by the simulation. The method proposed by Selvan et al. [32] has been used to determine the arc core radius from the electric current density. A line probe was used to extract the electric current density in the x direction at the center of the inter-electrode gap, and the values have been plotted in Fig. 18. The arc diameter is defined as the distance between the two points where the electric current density reaches 10% of the maximum values. Using this approach, the arc core radius was estimated to be 0.163 mm. This arc core radius estimation compares well with the value shown by Rohani et al. [33] which was between 0.15 and 0.16 mm. The estimated arc core radius of 0.163 mm agrees with the isothermal plasma sphere radius (R_p= 1 mm) order of magnitude chosen for the NEC computation.

VI. DISCUSSION

The improvement with respect to the Lebouvier et al. [1] model is represented by the electrical characterization of the electrodes in the form a sheath model, the improved thermodynamic and [29] transport properties from the *EquilTheTA* tool, and the NEC being specified at the individual operating pressures. Although the electric potential at the cathode tip from this study is 38% greater than Lebouvier et al. [1], the value is still 14% lower than experimental data at 8 MPa.

The coefficients used in the empirical formula proposed by Rümpler [12] were calculated for a gas at atmospheric pressure. Therefore, further improvement could be obtained by refining the sheath model inputs at high pressure to calculate more accurate cathode electric potential. Benilov [31, 34] presented a review on the consideration of electrode interaction in arc discharges at high pressure. However, data for voltage drop near the electrodes at high pressure and low current are rarely measured and reported in literature.

The arc temperature evolution shows the arc sliding motion along the anode and bending motion towards the top of the

© 2022 IEEE. Personal use is permitted, but republication/redistribution requires IEEE permission. See https://www.ieee.org/publications/rights/index.html for more information.

This article has been accepted for publication in IEEE Transactions on Plasma Science. This is the author's version which has not been fully edited and content may change prior to final publication. Citation information: DOI 10.1109/TPS.2022.3193348

reactor at a physical time of 50 ms. The natural convection flow towards the top of the reactor is evident and represents the reason of the arc bending.

The convection effects can be observed in the velocity field evolution. The Helium gas is subjected to natural convection resulting in a low velocity magnitude with the gas moving towards the top of the reactor.

A validated CFD result of the plasma arc discharge has been obtained by comparing the results of this study against experimental measurements. The model was developed assuming Local Thermodynamic Equilibrium (LTE), therefore a thermal plasma was modelled. Non-thermal effects could be included in future developments when the plasma chemistry is considered for gases such as air and oxygen.

VII. Conclusions

The aim of this paper was to validate our numerical model developed using *Simcenter STAR-CCM+ version 2021.1* with respect to the experimental results, which was previously generated from our research group. The results were presented at operating pressures of 2, 4, 6, and 8 MPa, with more focus on the plasma behavior at 8 MPa. To try and improve our model in comparison to a previous study in literature, the thermodynamics and transport properties were upgraded using the *EquilTheTA* tool to better estimate the effects of high pressures. Thereafter, the model considered the effect of electrode interactions by taking into account the sheath model which is not considered in a previous study in literature [1].

Hence, this study show that the differences between our modelling approach in comparison to the previous study in literature by Lebouvier et al. [1] has a significant improvement on electric potential. Finally, our study highlights the importance of thermodynamic properties and transport coefficients deviation at higher pressure and temperatures greater than 10000 K, and the contribution of the sheath model.

VIII. References

1. Lebouvier A, Iwarere SA, Ramjugernath D, Fulcheri L. 3D magnetohydrodynamic modelling of a dc low-current plasma arc batch reactor at very high pressure in helium. Journal of Physics D: Applied Physics. 2013;46(14):145203.
2. Murphy AB. Transport coefficients of helium and argon-helium plasmas. IEEE Transactions on Plasma Science. 1997;25(5):809-14.
3. Colonna G, D'Angola A. EquilTheTA: Thermodynamic and Transport Properties of Complex Equilibrium Plasmas. AIP Conference Proceedings. 2012;1501.
4. D'Angola A, Colonna G, Gorse C, Capitelli M. Thermodynamic and transport propertiesin equilibrium air plasmas in a wide pressure and temperature range. The European Physical Journal D. 2008;46(1):129-50.
5. D'Angola A, Colonna G, Gorse C, Capitelli M. Thermodynamic properties of high temperature air in local thermodynamic equilibrium: II accurate analytical expression for electron molar fractions. The European Physical Journal D. 2011;65:453-7.
6. Colonna G, D'Angola A, Pietanza LD, Capitelli M, Pirani F, Stevanato E, et al. Thermodynamic and transport properties of plasmas including silicon-based compounds. Plasma Sources Science and Technology. 2018;27(1):015007.
7. Colonna G, D'Angola A, Laricchiuta A, Bruno D, Capitelli M. Analytical Expressions of Thermodynamic and Transport Properties of the Martian Atmosphere in a Wide Temperature and Pressure Range. Plasma Chemistry and Plasma Processing. 2013;33:401.
8. D'Angola A, Colonna G, Bonomo A, Bruno D, Laricchiuta A, Capitelli M. A phenomenological approach for the transport properties of air plasmas. The European Physical Journal D. 2012;66:205.
9. Colonna G, D'Angola A. A hierarchical approach for fast and accurate equilibrium calculation. Computer Physics Communications. 2004;163(3):177-90.
10. Cressault Y, Rouffet ME, Gleizes A, Meillot E. Net emission of Ar–H2–He thermal plasmas at atmospheric pressure. Journal of Physics D: Applied Physics. 2010;43(33):335204.
11. Salem D, Hannachi R, Cressault Y, Teulet P, Béji L. Radiative properties of argon–helium–nitrogen–carbon–cobalt–nickel plasmas used in CNT synthesis. Journal of Physics D: Applied Physics. 2015;48(6):065202.
12. Rümpler C. Lichtbogensimulation für Niederspannungsschaltgeräte [PhD]. Ilmenau, Germany: Techn. Univers. Ilmenau, Germany; 2009.
13. Siemens. Simcenter STAR-CCM+ 2020.1.1 User Manual - Build 15.02.009 (win64/intel18.3vc14-r8 Double Precision): Siemens PLM Software; 2020.
14. Freton P, Gonzalez J-J, Escalier G. Prediction of the cathodic arc root behaviour in a hollow cathode thermal plasma torch. Journal of Physics D: Applied Physics. 2009;42(19):195205.
15. Jin Myung P, Keun Su K, Tae Hyung H, Sang Hee H. Three-dimensional modeling of arc root rotation by external magnetic field in nontransferred thermal plasma torches. IEEE Transactions on Plasma Science. 2004;32(2):479-87.
16. Gupta RN, Lee K-P, Thompson RA, Yos JM. Calculations and Curve Fits of Thermodynamic and Transport Properties for Equilibrium Air to 30 000 K. National Aeronautics and Space Administration (NASA); 1991.
17. Bernardi D, Colombo V, Coppa GGM, D'Angola A. Simulation of the ignition transient in RF inductively-coupled plasma torches. The European Physical Journal D. 2001;14:337-48.
18. Chinè B, editor A 2D Model of a Plasma Torch. COMSOL Conference; 2016; Munich.
19. Chinè B, editor A Plasma Torch Model. COMSOL Conference; 2017; Rotterdam.
20. Fuchs R, Murmann M, Nordborg H, editors. Towards an Efficient Arc Simulation Framework2017.
21. Landshoff RKM, Magee JL. Thermal Radiation Phenomena. New York: SpringerLink; 1969.
22. Bartlova M, Aubrecht V, Coufal O. Net Emission Coefficients Of Radiation In Thermal Plasmas Of Air With Carbon Admixture. Publications de l'Observatoire Astronomique de Beograd. 2010.

© 2022 IEEE. Personal use is permitted, but republication/redistribution requires IEEE permission. See https://www.ieee.org/publications/rights/index.html for more information.

This article has been accepted for publication in IEEE Transactions on Plasma Science. This is the author's version which has not been fully edited and content may change prior to final publication. Citation information: DOI 10.1109/TPS.2022.3193348

23. Aubrecht V, Bartlova M, Coufal O. Radiative emission from air thermal plasmas with vapour of Cu or W. Journal of Physics D: Applied Physics. 2010;43(43):434007.
24. Lowke JJ. Predictions of arc temperature profiles using approximate emission coefficients for radiation losses. Journal of Quantitative Spectroscopy and Radiative Transfer. 1974;14(2):111-22.
25. Billoux T, Cressault Y, Teulet P, Gleizes A. Calculation of the net emission coefficient of an air thermal plasma at very high pressure. Journal of Physics: Conference Series. 2012;406:012010.
26. Yokomizu Y, Matsumura T, Sun WY, Lowke JJ. Electrode sheath voltages for helium arcs between non-thermionic electrodes of iron, copper and titanium. Journal of Physics D: Applied Physics. 1998;31(7):880-3.
27. Mentel J, Luhmann J, Nandelstadt D, editors. Experimental investigation of electrodes for high pressure discharge lamps. Conference Record of the 2000 IEEE Industry Applications Conference Thirty-Fifth IAS Annual Meeting and World Conference on Industrial Applications of Electrical Energy (Cat No00CH37129); 2000 8-12 Oct. 2000.
28. Roth JR. Industrial plasma engineering. Vol.1, Principles. Bristol ;: Institute of Physics Pub.; 1995.
29. Fulcheri L, Rohani V, Fabry F, Traisnel N. Experimental electrical characterization of a low-current tip–tip arc discharge in helium atmosphere at very high pressure. Plasma Sources Science and Technology. 2010;19(4):045010.
30. Lawson SJ, Woodgate M, Steijl R, Barakos GN. High performance computing for challenging problems in computational fluid dynamics. Progress in Aerospace Sciences. 2012;52:19-29.
31. Benilov MS. Understanding and modelling plasma–electrode interaction in high-pressure arc discharges: a review. Journal of Physics D: Applied Physics. 2008;41(14):144001.
32. Selvan B, Ramachandran K, Sreekumar KP, Thiyagarajan TK, Ananthapadmanabhan PV. Three-Dimensional Numerical Modeling of an Ar-N2 Plasma Arc Inside a Non-Transferred Torch. Plasma Science and Technology. 2009;11:679.
33. Rohani V, Iwarere S, Fabry F, Mourard D, Izquierdo E, Ramjugernath D, et al. Experimental Study of Hydrocarbons Synthesis from Syngas by a Tip–Tip Electrical Discharge at Very High Pressure. Plasma Chemistry and Plasma Processing. 2011;31(5):663.
34. Li H-P, Benilov MS. Effect of a near-cathode sheath on heat transfer in high-pressure arc plasmas. Journal of Physics D: Applied Physics. 2007;40(7):2010-7.

IX. FIGURES

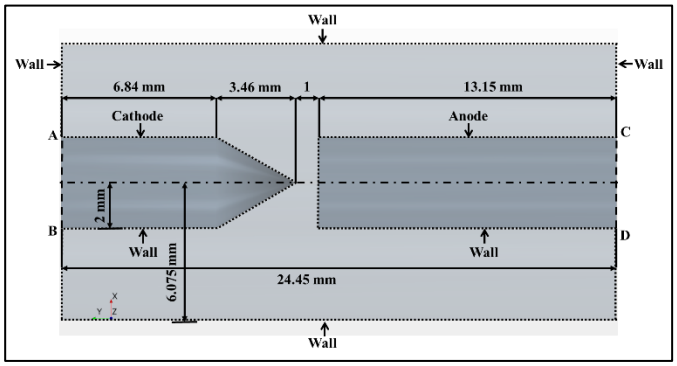

Fig. 1. A two-dimensional view of the high pressure plasma reactor.

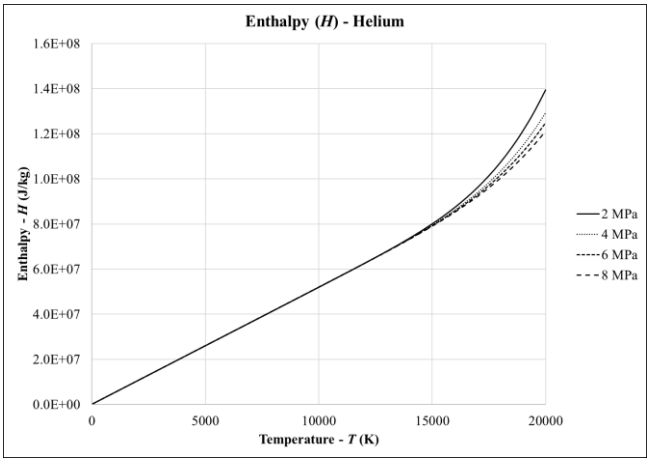

Fig. 2. Enthalpy of Helium at high pressure as a function of temperature.

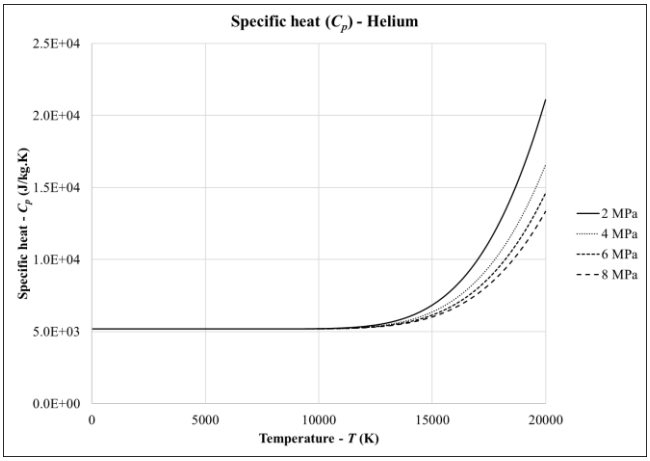

Fig. 3. Specific heat (at constant pressure) of Helium at high pressure as a function of temperature.

© 2022 IEEE. Personal use is permitted, but republication/redistribution requires IEEE permission. See https://www.ieee.org/publications/rights/index.html for more information.

This article has been accepted for publication in IEEE Transactions on Plasma Science. This is the author's version which has not been fully edited and content may change prior to final publication. Citation information: DOI 10.1109/TPS.2022.3193348

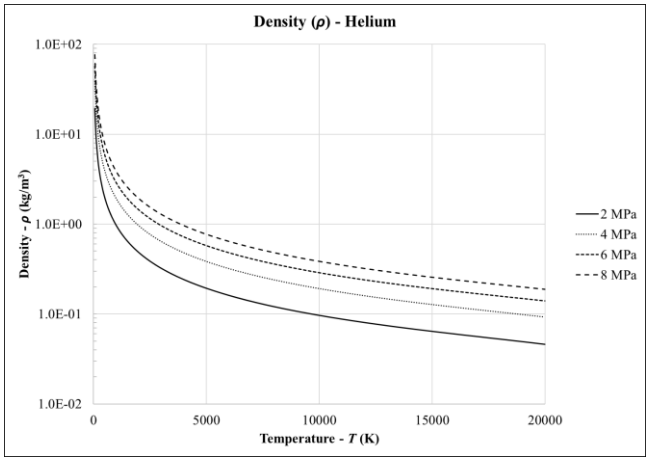

Fig. 4. Density of Helium at high pressure as a function of temperature.

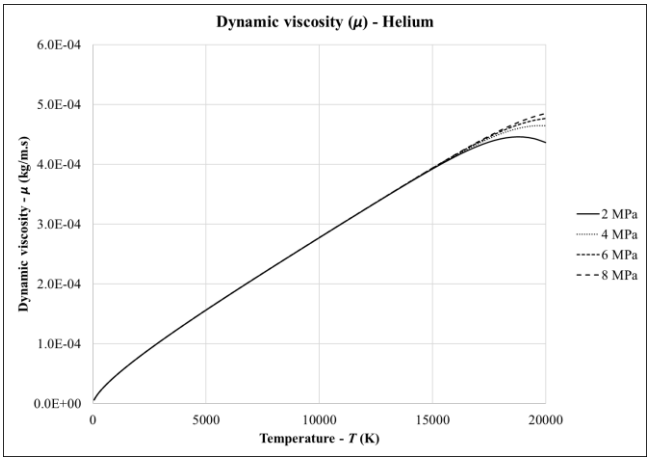

Fig. 7. Dynamic viscosity of Helium at high pressure as a function of temperature.

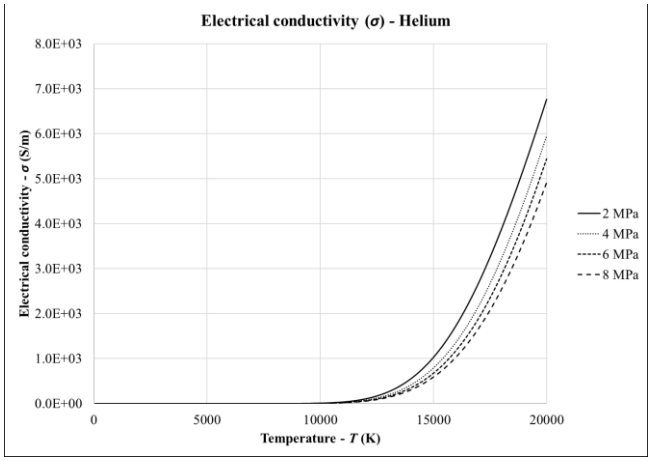

Fig. 5. Electrical conductivity of Helium at high pressure as a function of temperature.

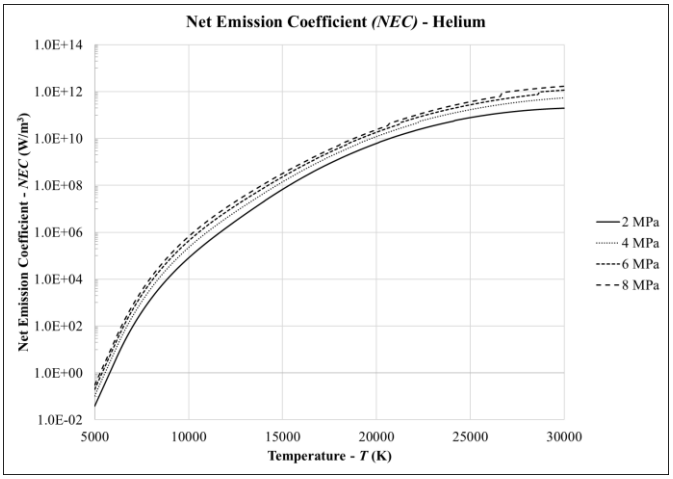

Fig. 8. Net Emission Coefficient data for Helium at high pressure as a function of temperature ($\boldsymbol{R_p}$ = 1 mm).

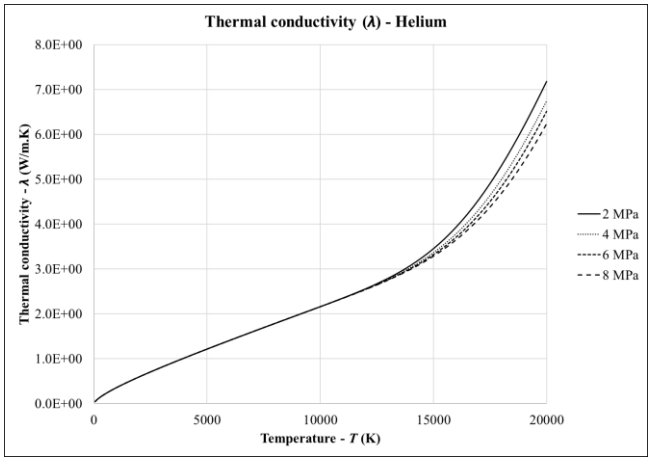

Fig. 6. Thermal conductivity of Helium at high pressure as a function of temperature.

© 2022 IEEE. Personal use is permitted, but republication/redistribution requires IEEE permission. See https://www.ieee.org/publications/rights/index.html for more information.

This article has been accepted for publication in IEEE Transactions on Plasma Science. This is the author's version which has not been fully edited and content may change prior to final publication. Citation information: DOI 10.1109/TPS.2022.3193348

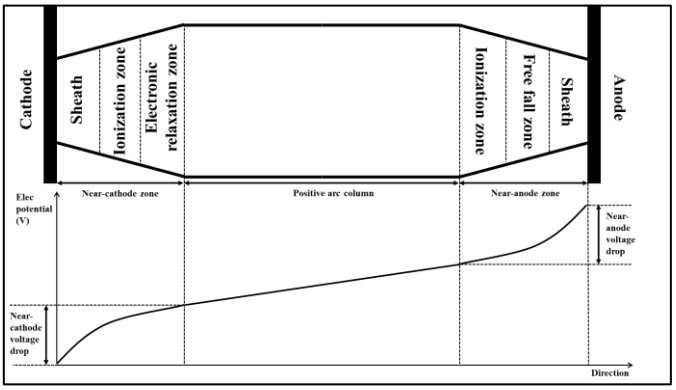

Fig. 9. The representation of an arc discharge and the axial variation of the voltage drop for each zone. Derived from Fulcheri et al. [29] and Roth [28].

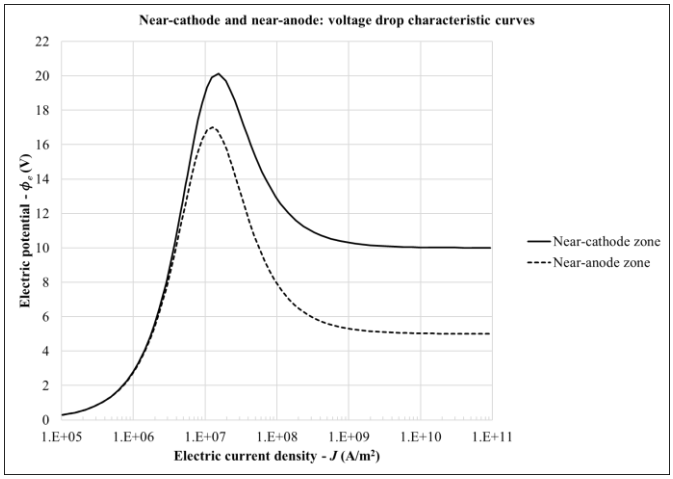

Fig. 10. The near-cathode and near-anode zone voltage drop characteristics calculated using the equation and coefficients determined by Rümpler.

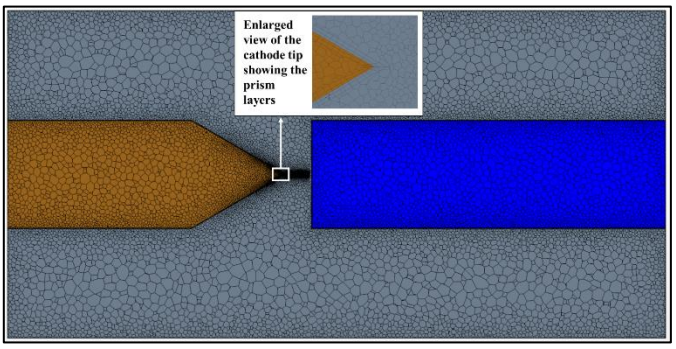

Fig. 11. The generated volume mesh with a total of 1 763 280 cells.

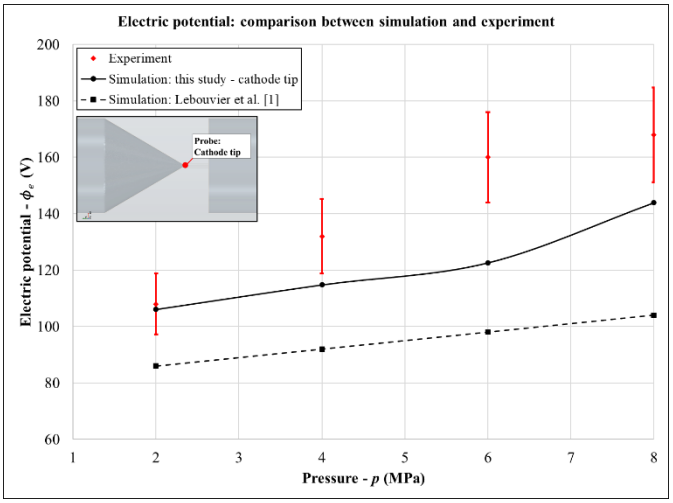

Fig. 12. Simulated voltage as a function of pressure being compared with experimental data ($\boldsymbol{I}$ = 0.35 A, $\boldsymbol{t}$ = 50 ms).

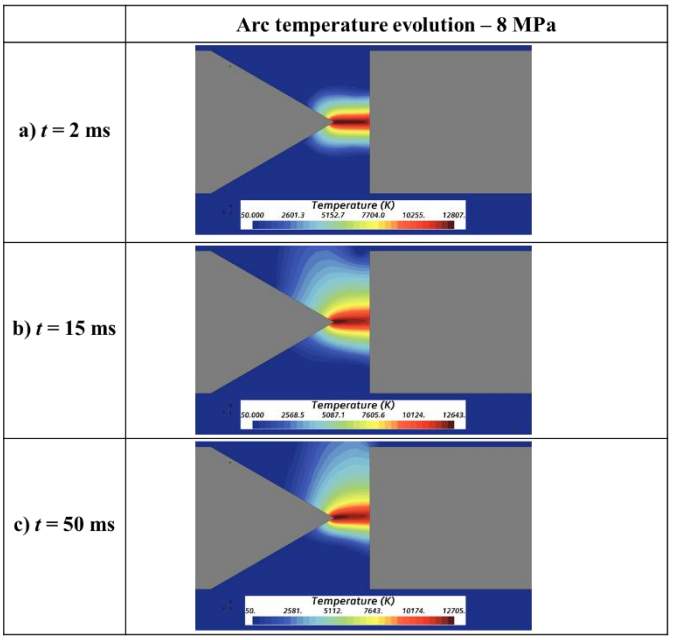

Fig. 13. The arc temperature evolution (p = 8 MPa).

© 2022 IEEE. Personal use is permitted, but republication/redistribution requires IEEE permission. See https://www.ieee.org/publications/rights/index.html for more information.

This article has been accepted for publication in IEEE Transactions on Plasma Science. This is the author's version which has not been fully edited and content may change prior to final publication. Citation information: DOI 10.1109/TPS.2022.3193348

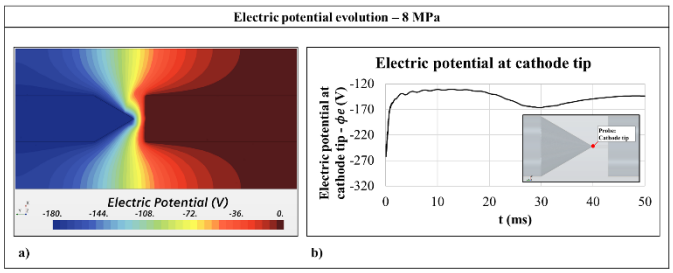

Fig. 14. a) Electric potential in the entire domain. b) Evolution of the electric potential at the cathode tip (p = 8 MPa).

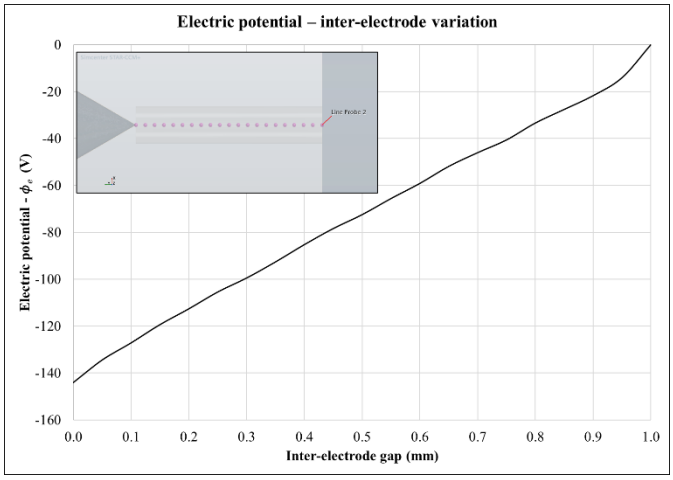

Fig. 15. The variation of the electric potential in the inter-electrode region (p =8 MPa).

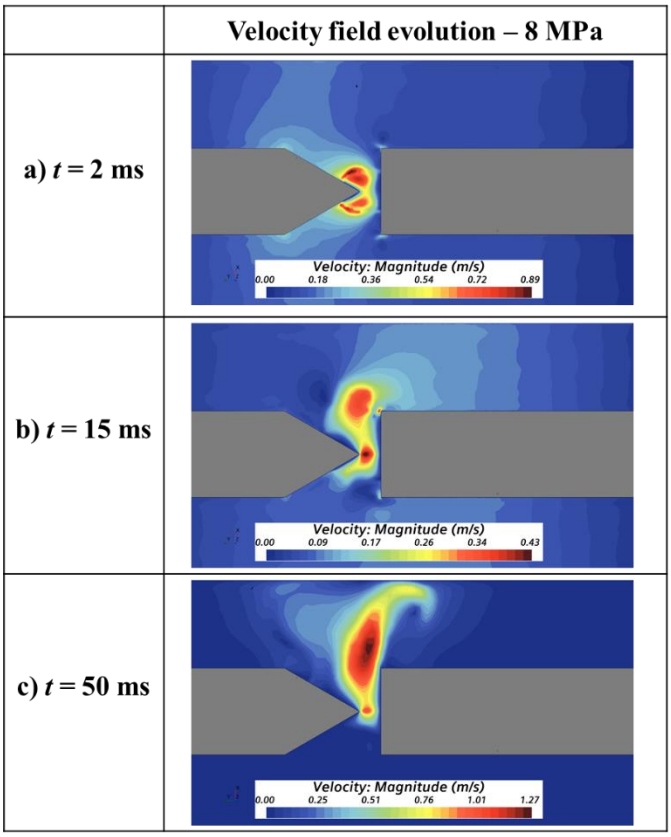

Fig. 16. The velocity field evolution (p = 8 MPa).

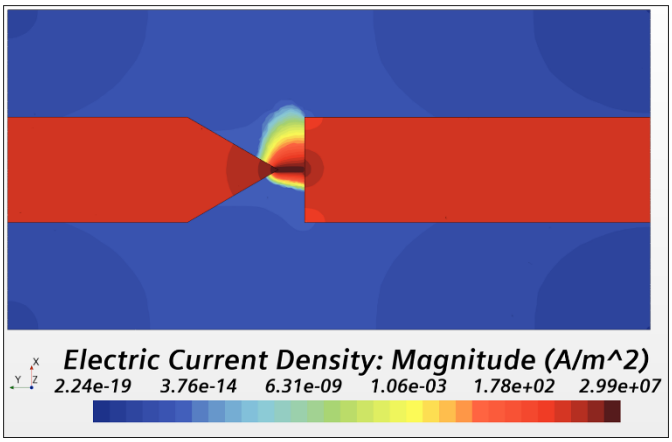

Fig. 17. The magnitude of the electric current density at t = 50 ms, (p = 8 MPa).

© 2022 IEEE. Personal use is permitted, but republication/redistribution requires IEEE permission. See https://www.ieee.org/publications/rights/index.html for more information.

This article has been accepted for publication in IEEE Transactions on Plasma Science. This is the author's version which has not been fully edited and content may change prior to final publication. Citation information: DOI 10.1109/TPS.2022.3193348

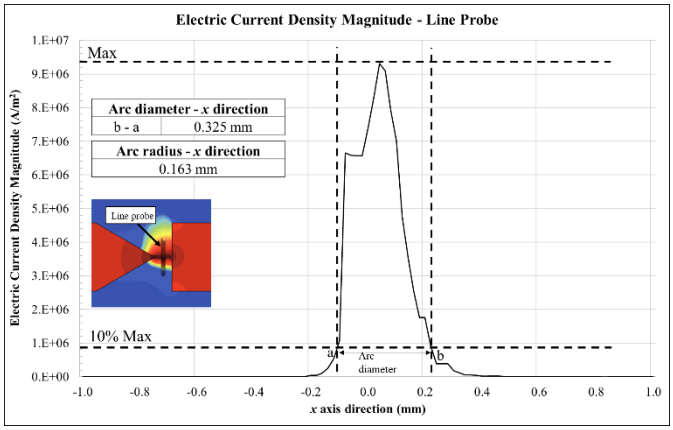

Fig. 18. The arc diameter estimated from a plot of the electric current density in the middle of the inter-electrode gap as a function of the *x* axis direction.

X. Tables

TABLE I. BOUNDARY CONDITIONS FOR THE MODEL

Parameter	Units	Walls	Cathode	Anode
v	m/s	0	0	0
T	K	$\frac{\partial T}{\partial n} = 0$	$\frac{\partial T}{\partial n} = 0$	$\frac{\partial T}{\partial n} = 0$
Electrodynamics	-	I = 0 A	I = -0.35A	$\bar{\phi}$ = 0 V
p	Pa	$\frac{\partial p}{\partial n} = 0$	$\frac{\partial p}{\partial n} = 0$	$\frac{\partial p}{\partial n} = 0$
$\mathbf{A}_{tangent}$	Wb/m	0	$\frac{\partial \mathbf{A}_{tangent}}{\partial n} = 0$	$\frac{\partial \mathbf{A}_{tangent}}{\partial n} = 0$

TABLE II. ELECTRODE BOUNDARY CONDITIONS

	Electric potential specification	Tangential magnetic vector potential $(\mathbf{A}_{tangent})$
Cathode boundary *AB*	I = -0.35 A	0 Wb/m
Cathode wall boundary	Insulator	0 Wb/m
Anode boundary *CD*	ϕ_e = 0 V	0 Wb/m
Anode wall boundary	Insulator	0 Wb/m

TABLE III. HELIUM WALL BOUNDARY CONDITIONS

	Method
Electric potential specification (ϕ)	Insulator
Magnetic vector potential $(\mathbf{A})$	$\mathbf{A}_{tangent}$ = 0 Wb/m
Shear stress specification	No-slip
Tangential velocity specification	Fixed
Thermal specification	Adiabatic

TABLE IV. COEFFICIENTS FOR NEAR-CATHODE AND NEAR ANODE VOLTAGE DROP EQUATION

Coefficient	Anode	Cathode
a	3.0E8	3.0E8
b	5.0	10
c	1.1E14	1.1E14
d	2.0	2.0

XI. Biographies

Avinash Maharaj (part-time PhD student, University of Kwa-Zulu Natal) obtained a Bachelor of Science in Engineering (Mechanical Engineering) degree from the University of KwaZulu-Natal, Durban, South Africa in 2010. He next obtained a Master of Science in Engineering degree from the University of the Witwatersrand, Johannesburg, South Africa in 2014.

He began his career working as a Process Engineer in the energy sector focusing on fossil fuel power plants. He is currently pursuing his PhD degree on a part-time basis and works as a Consulting Engineer in the built environment industry in Durban, South Africa. His research interests are in the field of plasma modelling using Computational Fluid Dynamics (CFD).

Mr. Maharaj is registered as a Professional Engineer with the Engineering Council of South Africa (ECSA).

Oleg Kazak (Application Engineer in Plasma Physics, Siemens Industries Software) obtained a Master of Physics degree from the Donetsk National University, Donetsk, Ukraine in 2008. He obtained a Ph.D. degree at the Institute of Hydromechanics of NAS, Kyiv, Ukraine (mechanics of liquids, gases, and plasma) in 2012. He is currently working as Application Engineer in areas related to Computational Electromagnetics, Plasma Physics and Magnetohydrodynamics, Heat Transfer and Radiation for the CFD software tool Simcenter STAR-CCM+. Previously he has worked as Engineer in eAircraft at Siemens, as PostDoc in

© 2022 IEEE. Personal use is permitted, but republication/redistribution requires IEEE permission. See https://www.ieee.org/publications/rights/index.html for more information.

This article has been accepted for publication in IEEE Transactions on Plasma Science. This is the author's version which has not been fully edited and content may change prior to final publication. Citation information: DOI 10.1109/TPS.2022.3193348

magnetohydrodynamic and electrical machines at Ilmenau University of Technology, Germany and PostDoc in Hydrodynamics at Ghent University, Belgium.

Angelo Limone (Technical Product Manager, Siemens Industries Software) obtained a Ph.D. degree at the University of Ulm and the Max Planck Institute for Plasma Physics, Germany. While contributing to this manuscript, he was working as Technical Product Manager in areas related to Low Frequency Computational Electromagnetics, Plasma Physics and Magnetohydrodynamics, CFD, Heat Transfer and Radiation for the CFD software tool *Simcenter STAR-CCM+*. Previously he has worked as Application Engineer in Plasma Physics at Siemens and as Computational Scientist at the ABB Corporate Research Centre, Switzerland.

Antonio D'Angola (Professor, School of Engineering, University of Basilicata, Italy) has received the Master Degree in Nuclear Engineering in 1996 and the Ph.D. in Energetics in 2000 both at Politecnico di Torino, Italy.

Since 2018 he is Associate Professor at the University of Basilicata in Nuclear Reactor Physics. The scientific activity and areas of interest are: numerical methods for the simulation of plasmas by using Particle-In-Cell and Monte Carlo codes, calculation of thermodynamic and transport properties of ionized plasmas for industrial and aerospace applications, kinetic and fluid dynamic investigation of non-neutral plasmas for ultra-high vacuum systems, design of plasma torch with high efficiency and the laser-plasma interaction for medical applications. He co-authored a book in the series "Fundamental Aspects of Plasma Chemical Physics" and co-edited a book for Institute of Physics, "Plasma Modeling: method and applications".

Prof. D'Angola is Associate Researcher at Consiglio Nazionale delle Ricerche, Istituto per la Fisica e Tecnologia dei Plasmi, ISTP.

Gianpiero Colonna (Senior Researcher, Consiglio Nazionale delle Ricerche, Istituto per la Fisica e Tecnologia dei Plasmi, ISTP) obtained Degree in Physics (1991) and PhD in Chemistry (1996) in the University of Bari, Italy.

After a PostDoc in University of British Columbia, became researcher in the University of Bari and in 1998, moved to the plasma institute of CNR. He published more than 200 papers on international journals and co-authored two books in the series "Fundamental Aspects of Plasma Chemical Physics" and co-edited two books for Institute of Physics: "Plasma Modeling: method and applications" and "Meteoroid Entry Physics". His research activities are in the field of plasma modeling, high enthalpy flows, plasma thermodynamics and transport properties.

Yann Cressault (professor, Universite of Toulouse III) received his Ph.D. degree in physics and plasma discharge engineering from Paul Sabatier University, Toulouse, France, in 2001.

After being Associate professor from 20004 to 2019, he is now Professor at the Toulouse Paul Sabatier University and develops his research with the LAPLACE Laboratory, Toulouse, France. His teaching activities are mainly focused on plasmas, electrotechnics, and electronics. More specifically, he develops both theoretical and experimental research on radiative transfer and on the transport properties of thermal plasmas in local thermodynamic equilibrium and in nonequilibrium state. His current research interests include the optimization of thermal plasmas processes with the presence of electric arcs (circuit breakers, plasma torches, plasma welding, plasma cutting, and arc furnace).

Dr. Cressault is a member of the French Association Arc Electrique and the French network Plasmas Froids.

Samuel Ayodele Iwarere (Senior Researcher and Royal Society FLAIR Fellow, University of Pretoria) obtained a Ph.D. degree in (Chemical Engineering) with training in the field of Plasma Technology from the Plasma Group at Mines ParisTech, Sophia Antipolis (now part of PSL Research University), France in collaboration with the University of KwaZulu-Natal in 2013.

He is currently a Senior Researcher in the Department of Chemical Engineering at the University of Pretoria. He is a recipient of the prestigious Future Leaders - African Independent Research (FLAIR) Fellowship, funded by the UK Government as part of the Global Challenge Research Fund through the Royal Society. He is an Honorary Research Fellow at the University of KwaZulu-Natal acting in a supervisory role for PhD research. His current research activities involve plasma modeling and simulation, plasma environmental-related applications, and solid waste valorization.

© 2022 IEEE. Personal use is permitted, but republication/redistribution requires IEEE permission. See https://www.ieee.org/publications/rights/index.html for more information.